Ahnak1 modulates L-type Ca(2+) channel inactivation of rodent cardiomyocytes

Julio L. Alvarez, Daria Petzhold, Ines Pankonien, Joachim Behlke, Michiyoshi Kouno, Guy Vassort, Ingo Morano and Hannelore Haase

Ahnak1 modulates L-type Ca^{2+} channel inactivation of rodent cardiomyocytes

Julio L. Alvarez [2], Daria Petzhold [1], Ines Pankonien [1,3], Joachim Behlke [1], Michiyoshi Kouno[4], Guy Vassort [5], Ingo Morano [1,3], Hannelore Haase [1]

[1]Max Delbrück Center for Molecular Medicine (MDC), Berlin, Germany;

[2]Laboratorio de Electrofisiologia, Instituto de Cardiologia y Cirugia Cardiovascular, La Habana, Cuba;

[3]University Medicine Charité, Berlin, Germany;

[4]Department of Social and Environmental Medicine, Osaka University, Osaka, Japan;

[5]Physiopathologie Cardiovasculaire, INSERM U-637, Montpellier Cedex 5, France.

Key words: Ahnak1-deficient mice, recombinant ahnak1 C-terminus, calcium current kinetics, calcium channel beta2 subunit

Corresponding author:

Dr. Hannelore Haase

Max Delbrück Center für Molekulare Medizin (MDC)

Robert-Rössle-Str. 10

D-13092 Berlin, Germany

Tel.: ++49-30-9406-3483; Fax: ++49-30-9406-2579

Email: haase@mdc-berlin.de

Abstract

Ahnak1, a giant 700-kDa protein, has been implicated in Ca^{2+} signalling in various cells. Previous work suggested that the interaction between ahnak1 and $Cav\beta_2$ subunit plays a role in L-type Ca^{2+} current (I_{CaL}) regulation. Here, we performed structure-function studies with the most C-terminal domain of ahnak1 (188 amino acids) containing a PxxP consensus motif (designated as 188-PSTP) using ventricular cardiomyocytes isolated from rats, wild-type mice (WT), and ahnak1-deficient mice. *In-vitro* binding studies revealed that 188-PSTP conferred high affinity binding to $Cav\beta_2$ (K_d ~60 nM). Replacement of proline residues by alanines (188-ASTA) decreased $Cav\beta_2$ affinity about 20-fold. Both 188-PSTP and 188-ASTA were functional in ahnak1-expressing rat and mouse cardiomyocytes during whole cell patch-clamp. Upon intracellular application they increased the net Ca^{2+} influx by enhancing I_{CaL} density and/or increasing I_{CaL} inactivation time course without altering voltage-dependency. Specifically 188-ASTA, which failed to affect I_{CaL} density, markedly slowed I_{CaL} inactivation resulting in a 50-70% increase in transported Ca^{2+} during a 0-mV depolarising pulse. Both ahnak1 fragments also slowed current inactivation with Ba^{2+} as charge carrier. By contrast, neither 188-PSTP nor 188-ASTA affected any I_{CaL} characteristics in ahnak1-deficient mouse cardiomyocytes. Our results indicate that the presence of endogenous ahnak1 is required for tuning the voltage-dependent component of I_{CaL} inactivation by ahnak1 fragments. We suggest that ahnak1 modulates the accessibility of molecular determinants in $Cav\beta_2$ and/or scaffolds selectively different β-subunit isoforms in the heart.

Introduction

Ahnak1 is a large protein of ~700-kDa implicated in many fundamental biological processes, such as Ca^{2+} signalling, plasma membrane repair, exocytosis, and blood-brain barrier function (1, 17, 26, 27, 33, 34, 36, 40). It was originally identified in human neuroblastoma cells (44) and skin epithelial cells (23). Ahnak1 is abundantly expressed in muscle cells where it locates to the inner side of the plasma membrane (15, 25). The ahnak1 protein contains three main structural regions: a relatively short globular N-terminus, a large central region of ~4300 amino acids consisting of multiple repeated units, and the C-terminal ~1000 amino acids (44).

Given ahnak´s role as scaffolding and signalling molecule, one would expect that targeted ablation of ahnak1 results in a severe phenotype. However, ahnak1-deficient mice are fertile and have a normal life span suggesting that ahnak1 is redundant in this model (31, 32). Komura et al. (31) proposed ahnak2 as candidate to compensate for the loss of function of ahnak1. Ahnak2 is also a large protein with a typical central repeat structure. The repeating units of ahnak1 and ahnak2 share homology while the N-terminal- and C-terminal regions show no similarities. Notably, the C-terminus of ahnak1 harbours a PxxP consensus motif known as potential interaction partner for sarc homology 3 (SH3) domain-containing proteins (38).

Ahnak1 belongs to the increasing number of intracellular proteins interacting with the Cavβ subunit of voltage-dependent Ca^{2+} channels (30). We previously showed that ahnak1 binds to the β_2-subunit of cardiac Cav1.2 channels and modulates the L-type Ca^{2+} current (I_{CaL}) in rat cardiomyocytes (2, 18, 25). In fact, the most C-terminal region of ahnak1 encompassing 188 amino acids emerged as a potent modulator of I_{CaL}. Intracellular application of this fragment during whole cell patch-clamp increased I_{CaL} density and slowed its inactivation time course (2). As a working hypothesis we suggested that a certain portion of β_2-subunits is functionally masked by ahnak1 and can be relieved by competition with ahnak1-derived peptides. This mechanism would result in an enhanced I_{CaL} as β-subunits are generally known to increase channel open probability besides their role in addressing α_{1C} to the sarcolemma (11). However, less is known to account for the slower inactivation kinetics following ahnak peptide application. A peptide competition mechanism could solely account for this effect if β_2-subunit isoforms are relieved (are more available) that slow channel inactivation like the lipid-

3

modified β_{2a} isoform (39). But this isoform is not believed to constitute the functional type of β_2-subunit in rat heart (28, 46, 47).

In general, β-subunits belong to the protein family of membrane-associated guanylate kinases (MAGUK) comprising a SH3 and guanylate kinase (GK) element. It has been reported that in β-subunits the SH3 and GK elements form a functional important module that supports I_{CaL} and regulates channel inactivation (37). Thus, an alternative mechanism underlying slowing I_{CaL} inactivation can be envisioned if the C-terminal ahnak1 peptides applied through the patch pipette would directly bind to β_2-subunits or any other sites thereby influencing I_{CaL} gating. One can assume that the latter mode of action operates also in ahnak1-deficient cardiomyocytes.

In the present study we demonstrate that ahnak1 fragments failed to affect I_{CaL} in ahnak1-deficient cardiomyocytes, while they evoked an increase in Ca^{2+} entry in WT rodent cardiomyocytes preferentially by slowing I_{CaL} inactivation time course. Thus, ahnak1 plays a non-redundant role in L-type Ca^{2+} channel inactivation and provides a mechanism for tuning Ca^{2+} channel activity in the heart.

Materials and Methods

Recombinant proteins

The GST-tagged β_2-subunit (CaB2a, Oryctolagus cuniculus, NCBI Entry name gi|1498) was expressed and purified as described (25). The GST fusion protein containing the 188 C-terminal amino acids of ahnak1 (188-PSTP, previously designated as P3P4) was prepared as in (2). The proline residues corresponding to amino acid positions 5592 and 5595 in ahnak1 (Accession Number NP_001611) were substituted by alanine using the QuickChange site-directed mutagenesis kit (StratageneEurope, Amsterdam, Netherlands) to yield 188-ASTA. The GST fusion proteins containing the intracellular loops connecting domain I-II and II-III of the rabbit cardiac α_{1C} were expressed and purified using standard protocols. The pGEX constructs for these α_{1C}-containing fusion proteins were kindly provided by Dr. Nathan Dascal (Tel Aviv, Israel). All constructs were checked by restriction site mapping and sequencing.

Analytical ultracentrifugation

Equilibrium binding studies were performed in a XL-A type analytical ultracentrifuge (Beckman, Palo Alto, Ca, USA) equipped with UV absorbance optics as in (25). For data analysis the program POLYMOLE was used (4).

Surface plasmon resonance (SPR) binding

The purified recombinant proteins 188-PSTP and 188-ASTA were immobilized on a CM5 sensor chip (GE Healthcare, Uppsala, Sweden) at parallel flow cells by amine coupling according to manufacturer's instructions. The amount of proteins immobilized corresponded to approximately 700 response units (RU). An activated-deactivated surface without any immobilized protein was used as a control. SPR binding studies were performed at 25°C using a Biacore 2000 Instrument (GE Healthcare, Uppsala, Sweden). Purified GST-β_2-subunit was diluted in running buffer (50 mM Tris-HCl, 500 mM NaCl, pH 7.4). Different dilutions (2, 3, 4, and 5 µM) were injected into the flow cells at a rate of 20µl/min. After each run, the surface of the sensor chip was regenerated with a buffer consisting of 0.1% CHAPS, 0.1% TritonX 100, 0.1% Tween 20, 0.1% Tween 80, 333 mM NaCl, 16.6 mM NaOH until the baseline was reached. For data analyses, association rate constant k_{on} was calculated by local fitting using the BIAevaluation 3.2 RC 1 program (Biacore AB) and a single-site interaction (Langmuir) model whereby Chi^2 was below 5%. The analysis software corrects for systematic drift in baseline that occurred during measurements.

Tissue Sampling

A cohort of male ahnak1-deficient mice in a C57BL6/J genetic background and their WT controls were studied at 6 months of age if not stated otherwise. The generation of homozygous ahnak1-deficient mice was described in (32). Mice do not present any obvious abnormalities. They were maintained in a temperature-controlled environment with free access to standard laboratory chow and tap water in the animal facility of the Max Delbrück Center, Berlin, Germany. For cardiomyocytes preparations the animals were anaesthetized with isoflurane followed by intraperitoneal injection of 8

μg xylazine and 35 μg ketamine. The hearts were rapidly removed and processed as outlined below. Experiments were approved by the Berlin federal region´s institutional animal care body (LAGeSo T 0088/99).

Electrophysiological Measurements

Ventricular myocytes were isolated from adult male Wistar rats (200-300 g), from 6 months old male ahnak1-deficient mice and the respective wild-type littermates as in (2). The standard Tyrode solution was (mM): 117 NaCl, 4 KCl, 1.5 KH_2PO_4, 4.4 $NaHCO_3$, 1.7 $MgCl_2$, 10 HEPES, 10 glucose, pH 7.4. Collagenase (Worthington type CLS 2) was added at 0.8 mg/ml. The freshly dissociated cells were kept in the physiological solution with 1 mM Ca^{2+} and 0.5% bovine serum albumin at room temperature and used within 6-8 hours. L-type Ca^{2+} current (I_{CaL}) was recorded using the "whole-cell" variant of the patch-clamp method at room temperature (22 ± 2°C). 188-PSTP and 188-ASTA were directly dissolved in the pipette "intracellular" solution. Pipette tips were first immersed in the normal intracellular solution for at least 1 minute and then back filled with the intracellular solution containing the desired ahnak1 fragment. After gigaseal formation and rupture of the patch, cells were let to stabilize for at least 5 min before beginning the recordings. Ca^{2+} current density values were obtained after at least 10 min perfusion. Results were analysed by the Student's *t* test and are expressed as means ± SEM, * with p < 0.05. Further experimental details are given in Supplemental Material.

Heart tissue preparations

Tissue homogenates were prepared from frozen ventricular samples (100 mg) with 800 μl homogenization buffer consisting of (mM): 50 HEPES, 150 NaCl, 50 Na_2HPO_4, 25 NaF, 10 EDTA, 0.2 DTT, and protease inhibitor cocktails (Sigma P8340, Roche). The samples were first homogenized with a glass–teflon pestle and then with a Polytron PT 10-35 instrument at 10.000 rpm for 3 x 5 s. The cytosolic fraction was prepared by high-speed centrifugation (2 h at 100.000 x g) of the homogenates. Cardiac membrane fractions were prepared according to (29). Briefly, ventricular tissue (100 mg) was

homogenized twice with a KCl-containing (0.75 M) buffer to remove myofibrils followed by low salt

buffer including protease inhibitors as above.

Pull-down of endogenous β₂-subunits

The GST-fusion protein containing the intracellular loop connecting domain I-II of the rabbit cardiac

α_{1C} (2.5 µg) was bound to glutathione-sepharose (5 µl packed gel) in a final volume of 1 ml buffer A

consisting of 50 mM Tris, 150 mM NaCl, 0.2 % Triton X-100, 0.2 % CHAPS and protease inhibitor

cocktails (Sigma P8340, Roche), pH 7.4 for 1 h at 4°C on a rotating wheel. For control experiments,

the equimolar concentration of unfused GST protein was coupled under the same conditions. Cytosolic

fractions prepared from mouse and rat hearts (100 µg) were diluted with buffer A to a final volume of

1 ml and incubated with either α_{1C} I-II loop affinity beads or GST-control beads for 2 h at 4°C. The

beads were washed three times with 0.5 ml of buffer A for 5 min at 4°C, subsequently suspended in 60

µl SDS-sample buffer, and incubated for 3 min at 95°C.

Western-blot analyses

For ahnak1 detection, protein samples were separated on 6.5 % SDS-polyacrylamide gels and

transferred to nitrocellulose for 2 hours at 300 mA. For α_{1C}- and β_2-subunit detection, the protein

samples were separated on 8 % SDS-polyacrylamide gels and transferred for 90 min at 210 mA. The

transfers were incubated with affinity-purified antibodies (1 µg IgG/ml anti-ahnak1, 0.5 µg IgG/ml

anti-α_{1C}, 0.25 µg IgG/ml anti-β_2) followed by the peroxidase-coupled anti-rabbit IgG (dilution

1:100.000, Pierce, Rockford, IL, USA). Immunoreactive protein bands were visualized by the

enhanced chemiluminescence (ECL) reaction (Millipore). The anti-ahnak1 antibody was produced

against the head portion of ahnak1 as in [25]. The antigenic epitopes for anti-α_{1C} and anti-β_2 antibodies

comprised (EEEEKERKKLARTASPEKK) and (EWNRDVYIRQ), respectively [20, 41].

Results

The C-terminal -PxxP- motif in ahnak1 is important for high affinity β_2-subunit binding

The 5592-PSTP-5595 sequence in the C-terminal region of ahnak1 constitutes a PxxP consensus motif known to be important for protein-protein interaction (38). To study whether this motif plays a role for β_2-subunit interaction, we replaced the proline residues by alanine in a recombinant protein derived from ahnak1 encompassing the most C-terminal 188 amino acids and performed *in-vitro* binding studies. The ahnak1-derived proteins were designated as 188-PSTP and 188-ASTA, respectively throughout this study. Equilibrium binding experiments summarized in Figure 1A revealed remarkable differences in β_2-subunit binding. 188-PSTP displayed two-site β_2-subunit interaction with K_d values of 60 ± 20 nM (n=4) and 300 ± 100 nM (n=4) for high and low affinity sites, respectively. By contrast, 188-ASTA revealed a single population of binding sites with a K_d value of 1.2 ± 0.8 µM (n=8).

Next we studied protein-protein interaction within a minute time scale by surface plasmon resonance (SPR) spectroscopy. For these experiments 188-PSTP and 188-ASTA were covalently bound at neighboring lanes of a CM-5 biosensor chip at low ligand concentrations (700 RU corresponding to 0.7ng/mm^2). Subsequently, the chip was superfused with different concentrations of recombinant β_2-subunit followed by running buffer. Typical sensorgrams shown in Figure 1B illustrate that the β_2-subunit associates rapidly to both C-terminal ahnak1 fragments and dissociates slowly. The slow dissociation rates (particularly for 188-PSTP) observed in the concentration range tested (2µM to 5µM β_2-subunit) prevented the calculation of the Kd values from kinetic data ($Kd = k_{off}/k_{on}$). But, the association rate constants could well be estimated amounting to 2100 ± 300 M^{-1}s^{-1} (n=8) and 2400 ± 200 M^{-1}s^{-1} (n=8) for 188-PSTP and 188-ASTA, respectively. Together, the binding experiments prompted us to study *in-vivo* effects of these C-terminal ahnak1 fragments on cardiomyocytes.

Effects of 188-PSTP and 188-ASTA on Ca^{2+} currents of rat ventricular cardiomyocytes

Given the critical role of PSTP for β_2-subunit binding, we reasoned that 188-ASTA would be less efficient in I$_{CaL}$ modulation due to its lower affinity for the β_2-subunit. To address this question, we

applied 100-nM of one or the other ahnak1-fusion proteins to ventricular rat cardiomyocytes under patch clamp conditions. This concentration is well over the Kd value of the high affinity interaction site of the 188-PSTP/β_2 complex, but below the Kd value of the 188-ASTA/β_2 complex. Indeed, original traces depicted in Figure 2A illustrate that under these conditions 188-PSTP was sufficient to increase current amplitude by about 20% (from 10.8 ± 0.6 to 12.9 ± 0.8 pA/pF) and to prolong channel inactivation time course by significantly increasing the fast time constant, τ_{fast} (from 4.7 ± 02 to 5.5 ± 0.4 ms) leaving the slow component, τ_{slow} unaffected whereas 188-ASTA had no effect on I_{CaL} (data not shown). However, higher concentrations of 188-ASTA were functional. Figure 2B demonstrates an example for the application of 5-μM 188-ASTA (well over Kd) which led to a marked prolongation of the I_{CaL} inactivation time course by increasing both inactivation time constants τ_{fast} and τ_{slow} while peak current density remained unaffected. The increase in τ_{fast} by 100-nM 188-PSTP and the increases in both τ_{fast} and τ_{slow} by 5 μM 188-ASTA were not voltage-dependent as they occurred at all imposed membrane potentials (Figure 2C). No voltage-dependent shifts were observed on I_{CaL}-V and availability curves (data not shown). Together, although 188-PSTP and 188-ASTA affected I_{CaL} differently they led to a marked increase in the amount of transported charges (QCa^{2+}) during a 200-ms depolarization to 0 mV (Figure 2A, B, insets). When 188-PSTP and 188-ASTA were both applied at 10 μM, they increased QCa^{2+} by 59 % and 78 %, respectively (Table 1).

Changes in τ_{fast} have been commonly associated to the Ca^{2+}-dependent inactivation (CDI) mechanism. Hence, we asked whether the ahnak1 fragments are also functional when using Ba^{2+} as charge carrier. The results are summarized in Figure 3 and Table 1. Under control conditions in the presence of Ba^{2+}, peak inward current, I_{BaL} was increased ($\cong$60%) and inactivation time course markedly prolonged, as known. In the presence of 10-μM either 188-PSTP or 188-ASTA, I_{BaL} inactivation time constants were significantly increased to very similar extent while peak I_{BaL} was unaffected. The rise in τ_{fast} and τ_{slow} elicited by the ahnak1 fragments was not voltage-dependent (Figure 3B).

Effects of 188-PSTP and 188-ASTA on Ca^{2+} currents of mouse cardiomyocytes

To further understand the role of ahnak1 in Ca^{2+} current modulation, potential effects of the ahnak1 fragments on ahnak1-deficient (KO) cardiomyocytes were studied. We first examined the phenotype of ventricular myocytes isolated from KO mice. Western-blot analysis confirmed ahnak1 deficiency in KO myocytes (Figure 4A). Cardiomyocytes isolated from KO were shorter than those isolated from WT littermates (132.6 ± 1.8 μm, n=135 and 155.8 ± 2.2 μm, n= 155; in ahnak1-KO and WT, respectively). They showed regular cross-striation with similar mean resting sarcomere lengths (Figure 4B). In line with the reduced cell length, membrane capacitance values were significantly lower in KO myocytes (Table 2). KO cardiomyocytes displayed a lower I_{CaL} density at all investigated voltages (Figure 5A, Table 2). In addition, τ_{fast} was significantly smaller while τ_{slow} was not altered. Consequently, QCa^{2+} was smaller in ahnak1-deficient cardiomyocytes than in WT ones (Table 2). However, the activation and availability curves for the two cell types had similar slope factor and voltage-dependency as was suggested by the shape of I-V curves (Table 2).

Intracellular dialysis of WT cardiomyocytes with 10-μM 188-PSTP resulted in a 4 - 5 ms statistically significant increase in τ_{fast} of I_{CaL} while τ_{slow} and I_{CaL} density were not affected (Figure 6A, C). These effects of 188-PSTP represented a significant increase in QCa^{2+} from 0.33 ± 0.04 pC/pF to 0.41 ± 0.03 pC/pF. No changes were observed in I-V, activation and availability curves (data not shown). By contrast, intracellular dialysis of KO cardiomyocytes with 10-μM 188-PSTP had no effect on any I_{CaL} characteristics (Figure 6C, D).

In the next set of patch clamp experiments we investigated the effects of 10-μM 188-ASTA in WT mouse cardiomyocytes. 188-ASTA significantly increased both τ_{fast} and τ_{slow} in a voltage-independent fashion, leaving peak I_{CaL} unchanged (Figure 7A, C). This resulted in a significant increase in QCa^{2+} from 0.39 ± 0.01 pC/pF to 0.58 ± 0.04 pC/pF. Besides, intracellular dialysis of KO cardiomyocytes with 10-μM ASTA had no effects on any I_{CaL} characteristics (Figure 7B, D). Taken together, the C-terminal ahnak1 fragments require the presence of endogenous ahnak1 to affect I_{CaL} inactivation.

Ca^{2+} channel-subunit expression in the cardiac models

We asked whether the differences in I_{CaL} gating and modulation between ahnak1-KO and WT cardiomyocytes could be due to different expression levels of Ca^{2+} channel subunits. Western-blot analyses on cardiac membrane preparations revealed similar α_{1C} and β_2 protein levels in both strains (Figure 8A, B). Using recombinant proteins for calibration (Figure 8A, B, right panels), expression levels of ~2 pmoles and ~60 pmoles per mg of membrane protein were calculated for the endogenous L-type Ca^{2+} channel subunits α_{1C} and β_2, respectively (Table 3).

Next, we compared β_2-subunit expression in the two rodent models used for patch-clamp experiments. Consistent with previous reports (19-21) the prominent β_2 band migrated at 80-kDa in mouse and rat hearts. An additional faint β_2 signal was visible at 95-kDa in the rat. This band was more prominent in the cytosolic fraction and bound strongly to the α_{1C} I-II loop (Figure 8C). The latter finding defines the 95-kDa protein reliably as β_2-subunit isoform. Thus, species-specific differences were observed in isoform pattern and with respect to the distribution between membrane-bound and cytosolic β_2-subunits (Table 3).

Discussion

Our results show that upon intracellular delivery, the C-terminal ahnak1 fragments 188-PSTP and 188-ASTA enhance Ca^{2+} entry in non-transgenic, rodent cardiomyocytes mostly by slowing I_{CaL} inactivation. This gain-of-function effect was not observed in ahnak1-deficient cardiomyocytes. The data strongly suggest that ahnak1/Cavβ_2 complexes of control myocytes are targeted by ahnak1 fragments and imply that ahnak1 scaffolds different β_2-subunit isoforms.

Effects of 188-PSTP and 188-ASTA on L-type Ca^{2+} and Ba^{2+} currents

Equilibrium binding experiments revealed that the high affinity, two-site β_2-subunit interaction previously reported for a longer C-terminal ahnak1 fragment (25) is fully conserved within the 188 C-terminal amino acids. The mutations of PSTP into ASTA left intact only the lower affinity site with a K_d value around 1 μM, which is considered to be prone to physiological regulation. This interaction site was localized to the N-terminal portion of the Cavβ_2 including the SH3 domain (25). Real time

SPR binding measurements showed that both 188-PSTP and 188-ASTA associated rapidly with Cavβ_2. Although SPR experiments revealed no significant higher affinity for 188-PSTP, both *in-vitro* binding approaches suggested that the C-terminal ahnak1 fragments could interfere with Cavβ_2-regulated functions in cardiomyocytes. Indeed, our patch-clamp data clearly demonstrate that the ahnak1 fragments modify I_{CaL} inactivation time course in rat and mouse cardiomyocytes, but not in ahnak1-deficient cardiomyocytes. These results are indicative for a complex interaction involving at least three partners: ahnak1 fragments, Cavβ_2, and endogenous ahnak1.

The increases in both inactivation time constants, over 50% in τ_{fast}, led to significant increases in the amount of charges carried, QCa^{2+}. This observation is of physiological importance since most of Ca^{2+} entry (>75%) occurring during an action potential, particularly in rodents, is determined by the fast inactivation component of I_{Ca} (6). The modulation of I_{CaL} inactivation by C-terminal ahnak1 fragments that leads to a 50 - 70% change in QCa^{2+} in the first 30 msec, should have important effects on excitation-contraction coupling gain during an action potential if one further takes into account the existence of Ca^{2+} microdomains between the junctional sarcoplasmic reticulum and the T-tubular sarcolemma in which important increases in Ca^{2+} would be expected even in response to small changes in Ca^{2+} currents (6).

Inactivation of voltage-gated Ca^{2+} channels that serve as a major source of Ca^{2+} influx in excitable cells is precisely regulated. In the channel-forming α_{1C} subunit the C-terminal binding site for the Ca^{2+} sensor calmodulin appears essential for Ca^{2+}-dependent inactivation, CDI as well as the loop connecting domains I and II is essential for voltage-dependent inactivation, VDI. The molecular mechanisms of VDI remain poorly understood although predominant contributions arise from the β-subunits (see below). At first glance, replacing extracellular Ca^{2+} by Ba^{2+} easily separates the two processes, although to some extent CDI might result from a global change in intracellular Ca^{2+} occurring after Ca^{2+} release from internal stores (5). Furthermore VDI also exhibits fast and slow components (12, 13) which makes difficult to ascertain which one, CDI or fast VDI, predominates in the fast inactivation phase of I_{CaL} with Ca^{2+} as charge carrier. Interestingly, the CDI of Cav1.2 (cardiac L-type channel) and VDI of Cav2.1 (neuronal P/Q channel) are similarly regulated by the auxiliary β-

subunit (7, 8). Here we report that in rat and WT mouse 188-ASTA increases both τ_{fast} and τ_{slow} without shifting the voltage-dependence of the kinetics, nor altering the peak current amplitude. This increase in inactivation time constants is seen when using either Ca^{2+} or Ba^{2+} as the charge carrier. Furthermore in the presence of 188-PSTP, our results are just opposite to what is expected from a τ_{fast} - CDI paradigm since in rat cardiomyocytes, 188-PSTP increases peak I_{CaL} but slows down τ_{fast} (2). When Ba^{2+} equimolarly substitutes for Ca^{2+} as charge carrier, both fast and slow inactivation time constants of I_{BaL} are significantly increased by 188-PSTP and 188-ASTA. Under this condition L-type current inactivation is mostly due to a two-component VDI implying that ahnak1 fragments act mainly by modifying VDI through an interaction with the auxiliary β-subunit. However, other possibilities such as complex differential interactions of the permeating ion (Ca^{2+} or Ba^{2+}) with the voltage sensor cannot fully be ruled out (43).

Impact of Cavβ isoforms for channel inactivation

The differential effects of Cavβ isoforms on voltage-dependent inactivation are well documented. For example $Cav\beta_{2a}$ slows inactivation whereas other Cavβ isoforms accelerates it. Distinct structural determinants have been reported in Cavβ to account for these opposite actions including lipid-modification (9), membrane-attachment (45), and the GK domain (16). The paradigm "membrane-bound β_2 splice variants slow inactivation" was particularly extended by Herzig *et al.* (24), who showed that the degree of modulation correlates with the length of the amino-terminal domains of the β_2 splice variants in a manner that short N-termini (2a,b,e) slow inactivation while long N-termini (2c,2d) hasten inactivation. Of note recently two different missense mutations in $Cav\beta_{2b}$ have been reported to cause accelerated Ca^{2+} current inactivation underlying Brugada syndrome (3, 10). In light of our results, ahnak1 fragment-induced slowing of I_{CaL} could occur if that fragment applied through the patch pipette releases "slowing" Cavβ variants from endogenous ahnak1 and promotes their binding to I-II loop in Cav1.2 known to constitute the inactivating particle of the channel (39). To this end, there are no data available whether ahnak1 prefers a certain Cavβ isoform. Future studies should address this issue.

Alternatively, it can be envisioned that ahnak1 binding influences the accessibility of molecular determinants in Cavβ. Recently, Gonzalez-Gutierrez *et al.* (16) demonstrated that the GK domain present in all long Cavβ isoforms is the primary functional unit to slow I_{CaL} inactivation and masking this property allows for modulation. Although it is still a hypothesis we propose that ahnak1 scaffolds Cavβ in cardiomyocytes. It may contribute to functional compartmentalization of the various β-subunit isoforms identified in the heart (14, 22, 45) or may shape Cavβ subunits and thereby regulate the accessibility of molecular determinants. We found species-specific differences in $β_2$-subunit isoform pattern between rat and mouse hearts that are in line with the structural determinants for modifying I_{CaL} inactivation. In fact, I_{CaL} inactivation was relatively slow in mouse cardiomyocytes ($τ_{fast}$ ~13 ms) that showed a higher proportion of membrane-bound $β_2$-subunits. The I_{CaL} decay was very fast ($τ_{fast}$ ~5 ms) in rat cardiomyocytes that expressed a longer, cytosolic $β_2$-subunit isoform which likely represents the $Cavβ_{2c}$ (28). In both species we found overabundance of $β_2$-subunits compared to the channel forming $α_{1C}$, strengthening ahnak1 function as scaffold for $Cavβ_2$. The full-length ahnak1 molecule offers at least three attachments sites for the $β_2$-subunit utilizing ahnak1´s proximal and distal C-terminus (17).

Loss of I_{CaL} modulation by ahnak1 fragments in ahnak1-deficient cardiomyocytes

In agreement with previous reports, the ahnak1-deficient mice were fertile and had no evident abnormalities (31, 32). But, cardiomyocytes isolated from ahnak1-KO mice showed morphological and functional alterations compared to sex- and age-matched wild-type littermates. Ahnak1-deficient cardiomyocytes were smaller, particularly shorter consistent with the reduced cell capacitance. The reduction in cell length was not due to myocytes contraction as resting sarcomere distance was unaltered. Ahnak1-KO cardiomyocytes showed decreased I_{CaL} density and faster I_{CaL} inactivation kinetics. Reduced Ca^{2+} influx through I_{CaL} in ahnak1-deficient cardiomyocytes is in line with reports on ahnak1-deficient lymphocytes (35) and osteoblasts (42) suggesting that ahnak1 promotes membrane expression of functional Ca^{2+} channels. This conclusion is corroborated by unaltered

voltage-dependency of current-voltage relationship, activation, and availability curves of I_{CaL} in our KO myocytes.

The C-terminal ahnak1 fragments did not elicit any effects on I_{CaL} characteristics in ahnak1-deficient cardiomyocytes. These findings exclude the possibility that 188-PSTP or 188-ASTA bind to endogenous β_2-subunits or to any other site(s) and thereby influencing I_{CaL} gating. Furthermore, the loss of I_{CaL} modulation by ahnak1 fragments in ahnak1-deficient cardiomyocytes indicates that ahnak2 is not functional in this setting. Since ahnak2 lacks the C-terminal of ahnak1 it can not compensate for the loss of function of ahnak1. In all ahnak1-expressing cardiomyocytes, including WT littermates, 3-month old C57BL/6 mice (Alvarez, unpublished), 188-PSTP and 188-ASTA prolong I_{CaL} inactivation time course; however, 188-PSTP mostly affected τ_{fast} and only increased I_{CaL} density in rat (present results; (2). Our binding experiments can not explain the functional differences on I_{CaL} between 188-PSTP and 188-ASTA. Apparently, cross-talk with distinct counteracting sites on endogenous ahnak1 is required to affect different aspects of I_{CaL} gating.

Taken together, our results provide strong evidence for a non-redundant role of ahnak1 in the voltage-dependent inactivation of the cardiac L-type Ca^{2+} channel. The findings imply that ahnak1 scaffolds $Ca_\nu\beta$ isoforms and suggest the ahnak1/$Ca_\nu\beta$ interactions as target for tuning Ca^{2+} homeostasis in the heart.

References

1.   Alli AA, Gower WR, Jr. (2009) The C type natriuretic peptide receptor tethers AHNAK1 at the plasma membrane to potentiate arachidonic acid-induced calcium mobilization. Am J Physiol Cell Physiol 297:C1157-1167

2.   Alvarez J, Hamplova J, Hohaus A, Morano I, Haase H, Vassort G (2004) Calcium current in rat cardiomyocytes is modulated by the carboxyl-terminal ahnak domain. J Biol Chem 279:12456-12461

3.   Antzelevitch C, Pollevick GD, Cordeiro JM, Casis O, Sanguinetti MC, Aizawa Y, Guerchicoff A, Pfeiffer R, Oliva A, Wollnik B, Gelber P, Bonaros EP, Jr., Burashnikov E, Wu Y, Sargent JD, Schickel S, Oberheiden R, Bhatia A, Hsu LF, Haissaguerre M, Schimpf R, Borggrefe M, Wolpert C (2007) Loss-of-function mutations in the cardiac calcium channel underlie a new clinical entity characterized by ST-segment elevation, short QT intervals, and sudden cardiac death. Circulation 115:442-449

4.   Behlke J, Ristau O (1997) Molecular mass determination by sedimentation velocity experiments and direct fitting of the concentration profiles. Biophys J 72:428-434

5.   Benitah JP, Alvarez JL, Gomez AM (2009) L-type Ca(2+) current in ventricular cardiomyocytes. J Mol Cell Cardiol

6.   Bers DM (2008) Calcium cycling and signaling in cardiac myocytes. Annu Rev Physiol 70:23-49

7.   Cens T, Restituito S, Galas S, Charnet P (1999) Voltage and calcium use the same molecular determinants to inactivate calcium channels. J Biol Chem 274:5483-5490

8.   Cens T, Rousset M, Leyris JP, Fesquet P, Charnet P (2006) Voltage- and calcium-dependent inactivation in high voltage-gated Ca(2+) channels. Prog Biophys Mol Biol 90:104-117

9.   Chien AJ, Gao T, Perez-Reyes E, Hosey MM (1998) Membrane targeting of L-type calcium channels. Role of palmitoylation in the subcellular localization of the beta2a subunit. J Biol Chem 273:23590-23597

10.   Cordeiro JM, Marieb M, Pfeiffer R, Calloe K, Burashnikov E, Antzelevitch C (2009) Accelerated inactivation of the L-type calcium current due to a mutation in CACNB2b underlies Brugada syndrome. J Mol Cell Cardiol 46:695-703

11.   Dolphin AC (2003) Beta subunits of voltage-gated calcium channels. J Bioenerg Biomembr 35:599-620

12.   Ferreira G, Rios E, Reyes N (2003) Two components of voltage-dependent inactivation in Ca(v)1.2 channels revealed by its gating currents. Biophys J 84:3662-3678

13.   Findlay I (2004) Physiological modulation of inactivation in L-type Ca2+ channels: one switch. J Physiol 554:275-283

14. Foell JD, Balijepalli RC, Delisle BP, Yunker AM, Robia SL, Walker JW, McEnery MW, January CT, Kamp TJ (2004) Molecular heterogeneity of calcium channel beta-subunits in canine and human heart: evidence for differential subcellular localization. Physiol Genomics 17:183-200

15. Gentil BJ, Delphin C, Benaud C, Baudier J (2003) Expression of the giant protein AHNAK (desmoyokin) in muscle and lining epithelial cells. J Histochem Cytochem 51:339-348

16. Gonzalez-Gutierrez G, Miranda-Laferte E, Nothmann D, Schmidt S, Neely A, Hidalgo P (2008) The guanylate kinase domain of the beta-subunit of voltage-gated calcium channels suffices to modulate gating. Proc Natl Acad Sci U S A 105:14198-14203

17. Haase H (2007) Ahnak, a new player in beta-adrenergic regulation of the cardiac L-type Ca(2+) channel. Cardiovasc Res 73:19-25

18. Haase H, Alvarez J, Petzhold D, Doller A, Behlke J, Erdmann J, Hetzer R, Regitz-Zagrosek V, Vassort G, Morano I (2005) Ahnak is critical for cardiac Ca(V)1.2 calcium channel function and its beta-adrenergic regulation. Faseb J 19:1969-1977

19. Haase H, Kresse A, Hohaus A, Schulte HD, Maier M, Osterziel KJ, Lange PE, Morano I (1996) Expression of calcium channel subunits in the normal and diseased human myocardium. J Mol Med 74:99-104

20. Haase H, Pfitzmaier B, McEnery MW, Morano I (2000) Expression of Ca(2+) channel subunits during cardiac ontogeny in mice and rats: identification of fetal alpha(1C) and beta subunit isoforms. J Cell Biochem 76:695-703

21. Haase H, Podzuweit T, Lutsch G, Hohaus A, Kostka S, Lindschau C, Kott M, Kraft R, Morano I (1999) Signaling from beta-adrenoceptor to L-type calcium channel: identification of a novel cardiac protein kinase A target possessing similarities to AHNAK. Faseb J 13:2161-2172

22. Harry JB, Kobrinsky E, Abernethy DR, Soldatov NM (2004) New short splice variants of the human cardiac Cavbeta2 subunit: redefining the major functional motifs implemented in modulation of the Cav1.2 channel. J Biol Chem 279:46367-46372

23. Hashimoto T, Amagai M, Parry DA, Dixon TW, Tsukita S, Miki K, Sakai K, Inokuchi Y, Kudoh J, et al. (1993) Desmoyokin, a 680 kDa keratinocyte plasma membrane-associated protein, is homologous to the protein encoded by human gene AHNAK. J Cell Sci 105 (Pt 2):275-286

24. Herzig S, Khan IF, Grundemann D, Matthes J, Ludwig A, Michels G, Hoppe UC, Chaudhuri D, Schwartz A, Yue DT, Hullin R (2007) Mechanism of Ca(v)1.2 channel modulation by the amino terminus of cardiac beta2-subunits. Faseb J 21:1527-1538

25. Hohaus A, Person V, Behlke J, Schaper J, Morano I, Haase H (2002) The carboxyl-terminal region of ahnak provides a link between cardiac L-type Ca2+ channels and the actin-based cytoskeleton. Faseb J 16:1205-1216

26. Huang Y, Laval SH, van Remoortere A, Baudier J, Benaud C, Anderson LV, Straub V, Deelder A, Frants RR, den Dunnen JT, Bushby K, van der Maarel SM (2007) AHNAK, a novel component of the dysferlin protein complex, redistributes to the cytoplasm with dysferlin during skeletal muscle regeneration. Faseb J 21:732-742

27. Jaiswal JK, Marlow G, Summerill G, Mahjneh I, Mueller S, Hill M, Miyake K, Haase H, Anderson LV, Richard I, Kiuru-Enari S, McNeil PL, Simon SM, Bashir R (2007) Patients with a non-dysferlin Miyoshi myopathy have a novel membrane repair defect. Traffic 8:77-88

28. Kamada Y, Yamada Y, Yamakage M, Nagashima M, Tsutsuura M, Kobayashi T, Seki S, Namiki A, Tohse N (2004) Single-channel activity of L-type Ca2+ channels reconstituted with the beta2c subunit cloned from the rat heart. Eur J Pharmacol 487:37-45

29. Karczewski P, Bartel S, Krause EG (1990) Differential sensitivity to isoprenaline of troponin I and phospholamban phosphorylation in isolated rat hearts. Biochem J 266:115-122

30. Kobayashi T, Yamada Y, Fukao M, Tsutsuura M, Tohse N (2007) Regulation of Cav1.2 current: interaction with intracellular molecules. J Pharmacol Sci 103:347-353

31. Komuro A, Masuda Y, Kobayashi K, Babbitt R, Gunel M, Flavell RA, Marchesi VT (2004) The AHNAKs are a class of giant propeller-like proteins that associate with calcium channel proteins of cardiomyocytes and other cells. Proc Natl Acad Sci U S A 101:4053-4058
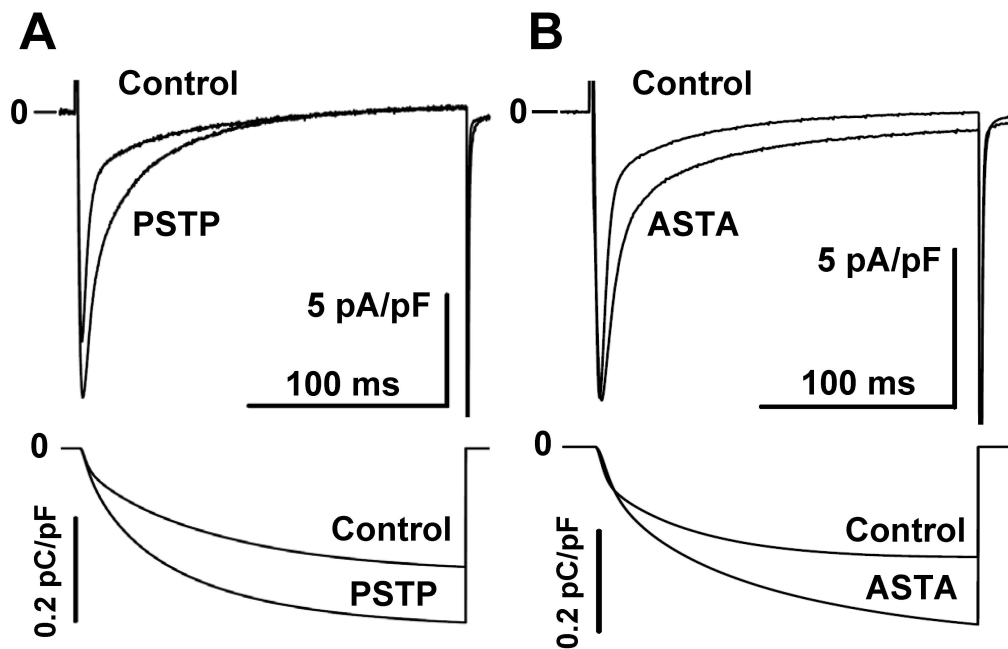
32. Kouno M, Kondoh G, Horie K, Komazawa N, Ishii N, Takahashi Y, Takeda J, Hashimoto T (2004) Ahnak/Desmoyokin is dispensable for proliferation, differentiation, and maintenance of integrity in mouse epidermis. J Invest Dermatol 123:700-707

33. Lee IH, Lim HJ, Yoon S, Seong JK, Bae DS, Rhee SG, Bae YS (2008) Ahnak protein activates protein kinase C (PKC) through dissociation of the PKC-protein phosphatase 2A complex. J Biol Chem 283:6312-6320

34. Lee IH, You JO, Ha KS, Bae DS, Suh PG, Rhee SG, Bae YS (2004) AHNAK-mediated activation of phospholipase C-gamma1 through protein kinase C. J Biol Chem 279:26645-26653

35. Matza D, Badou A, Kobayashi KS, Goldsmith-Pestana K, Masuda Y, Komuro A, McMahon-Pratt D, Marchesi VT, Flavell RA (2008) A scaffold protein, AHNAK1, is required for calcium signaling during T cell activation. Immunity 28:64-74

36. Matza D, Flavell RA (2009) Roles of Ca(v) channels and AHNAK1 in T cells: the beauty and the beast. Immunol Rev 231:257-264

37. McGee AW, Nunziato DA, Maltez JM, Prehoda KE, Pitt GS, Bredt DS (2004) Calcium channel function regulated by the SH3-GK module in beta subunits. Neuron 42:89-99

38. Nguyen JT, Turck CW, Cohen FE, Zuckermann RN, Lim WA (1998) Exploiting the basis of proline recognition by SH3 and WW domains: design of N-substituted inhibitors. Science 282:2088-2092

39. Restituito S, Cens T, Barrere C, Geib S, Galas S, De Waard M, Charnet P (2000) The [beta]2a subunit is a molecular groom for the Ca2+ channel inactivation gate. J Neurosci 20:9046-9052

40. Salim C, Boxberg YV, Alterio J, Fereol S, Nothias F (2009) The giant protein AHNAK involved in morphogenesis and laminin substrate adhesion of myelinating Schwann cells. Glia 57:535-549

41. Schotten U, Haase H, Frechen D, Greiser M, Stellbrink C, Vazquez-Jimenez JF, Morano I, Allessie MA, Hanrath P (2003) The L-type Ca2+-channel subunits alpha1C and beta2 are not downregulated in atrial myocardium of patients with chronic atrial fibrillation. J Mol Cell Cardiol 35:437-443
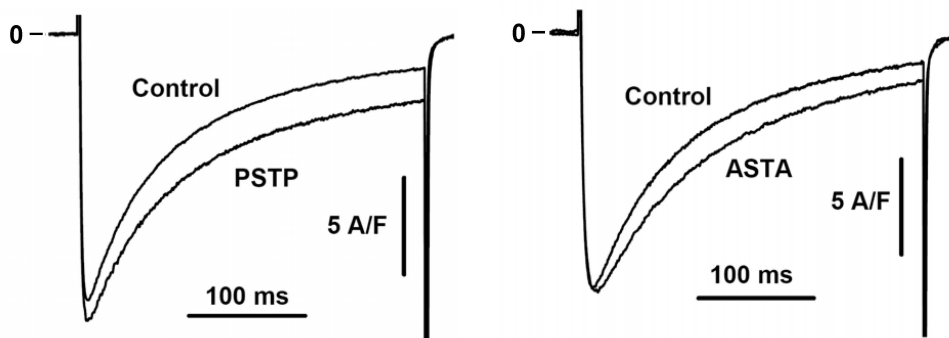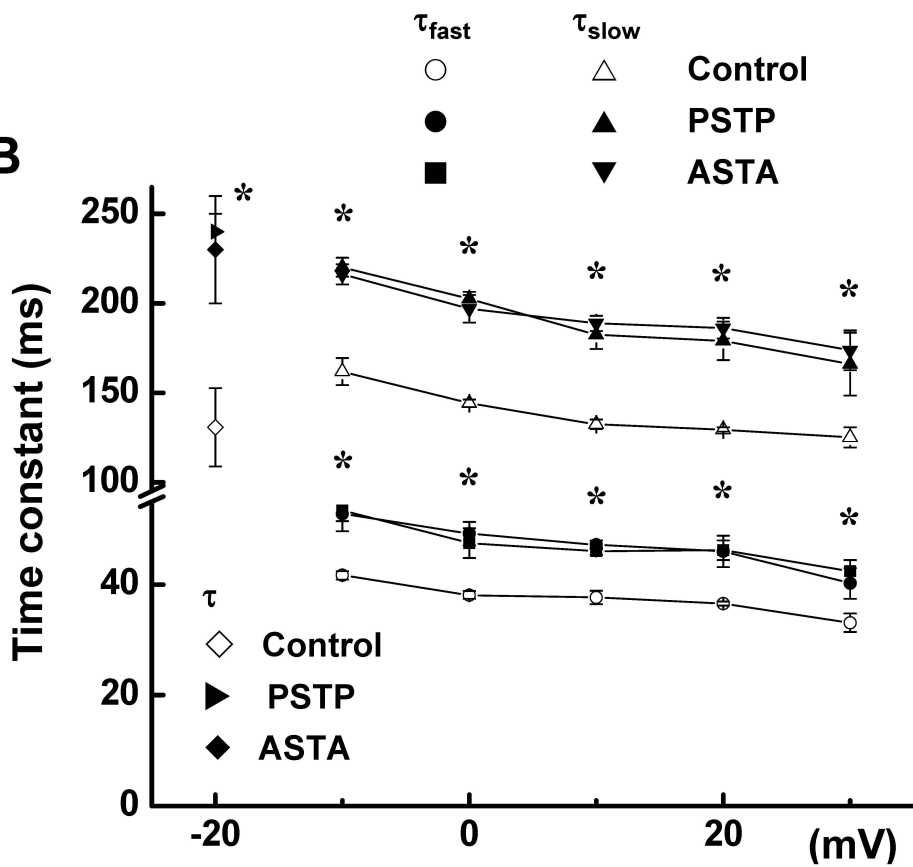
42.   Shao Y, Czymmek KJ, Jones PA, Fomin VP, Akanbi K, Duncan RL, Farach-Carson MC (2009) Dynamic interactions between L-type voltage-sensitive calcium channel Cav1.2 subunits and ahnak in osteoblastic cells. Am J Physiol Cell Physiol 296:C1067-1078

43.   Shirokov R (1999) Interaction between permeant ions and voltage sensor during inactivation of N-type Ca2+ channels. J Physiol 518 (Pt 3):697-703

44.   Shtivelman E, Cohen FE, Bishop JM (1992) A human gene (AHNAK) encoding an unusually large protein with a 1.2-microns polyionic rod structure. Proc Natl Acad Sci U S A 89:5472-5476

45.   Takahashi SX, Mittman S, Colecraft HM (2003) Distinctive modulatory effects of five human auxiliary beta2 subunit splice variants on L-type calcium channel gating. Biophys J 84:3007-3021

46.   Wei SK, Colecraft HM, DeMaria CD, Peterson BZ, Zhang R, Kohout TA, Rogers TB, Yue DT (2000) Ca(2+) channel modulation by recombinant auxiliary beta subunits expressed in young adult heart cells. Circ Res 86:175-184

47.   Yamada Y, Nagashima M, Tsutsuura M, Kobayashi T, Seki S, Makita N, Horio Y, Tohse N (2001) Cloning of a functional splice variant of L-type calcium channel beta 2 subunit from rat heart. J Biol Chem 276:47163-47170

A

B

A

	WT		Ahnak1-KO	
Ahnak1				
MyHC				
protein (µg)	20	40	20	40

B

WT

Ahnak1-KO

100 µm

A

MM (kDa)   Ahnak1-KO   Wild-type

Calibration
GST- β_2 subunit

95

72

cardiac membrane proteins
5 µg

0.1   0.5
pmoles

B

MM (kDa)   Ahnak1-KO   Wild-type

Calibration
GST- α1C II-III loop

250

cardiac membrane proteins
30 µg

0.1   0.5
pmoles

C

MM (kDa)   Mouse   Rat
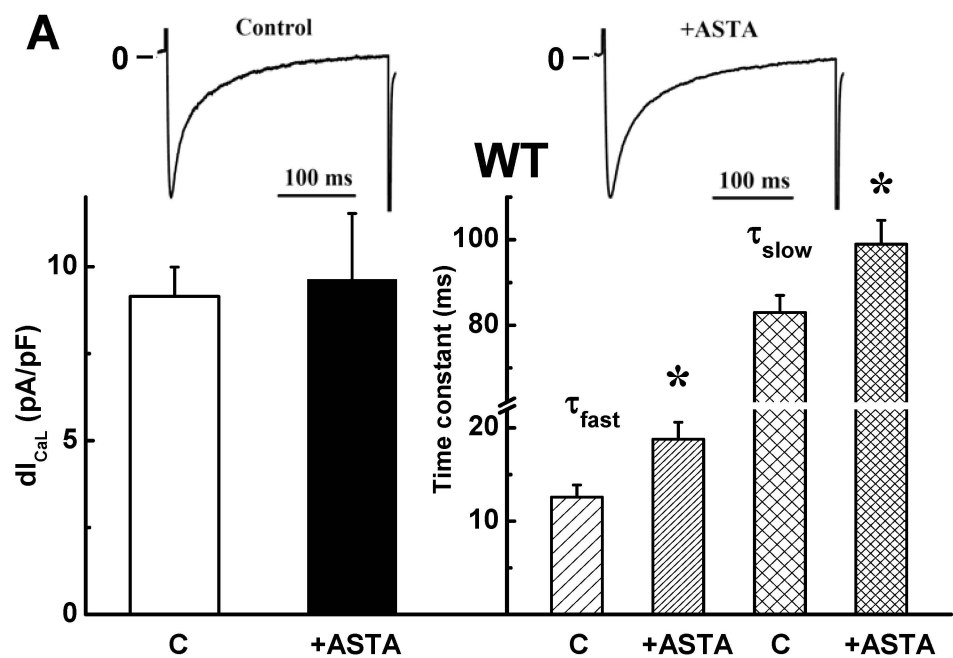
Rat Heart
Cytosol
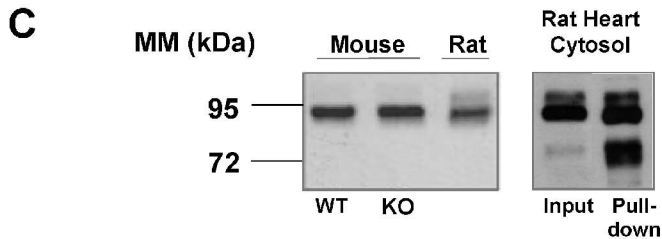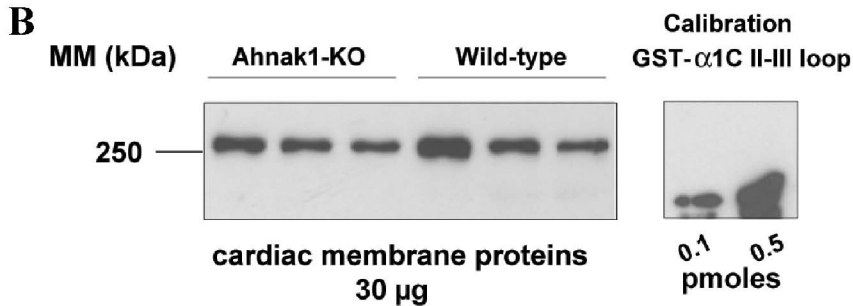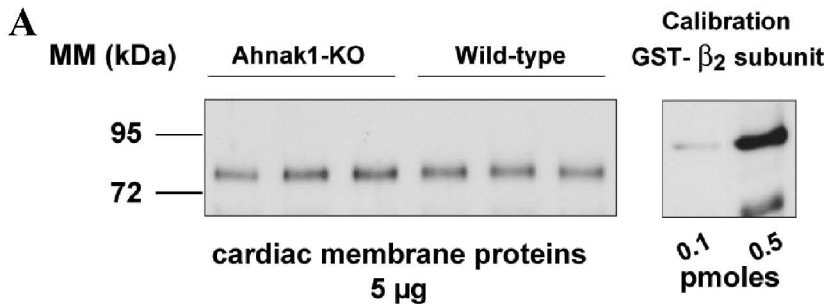
95

72

WT   KO

Input   Pull-down
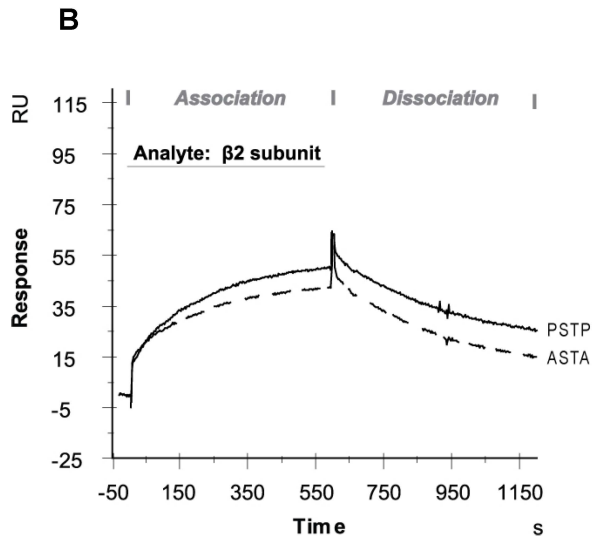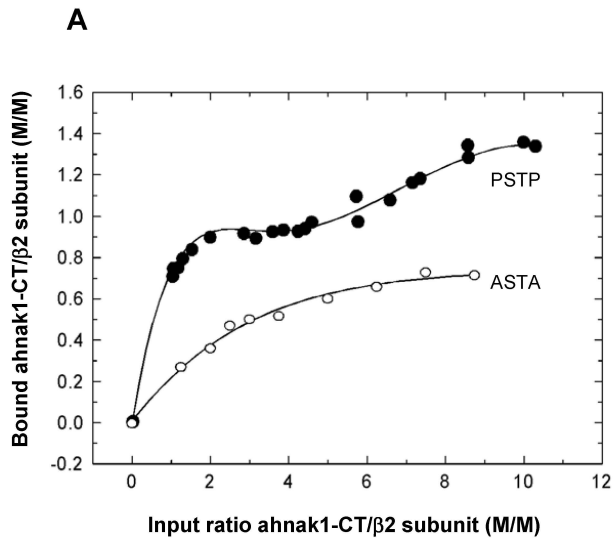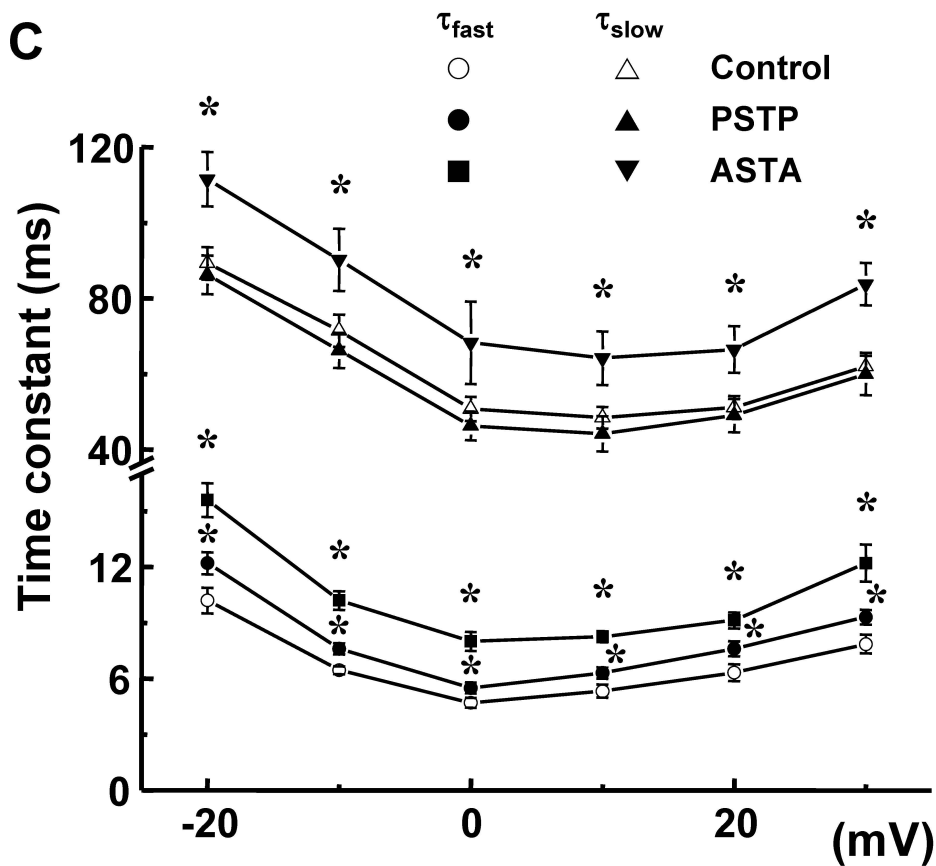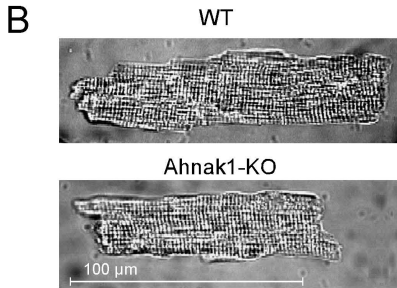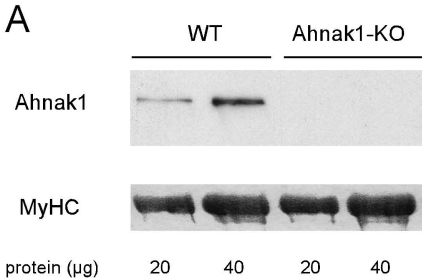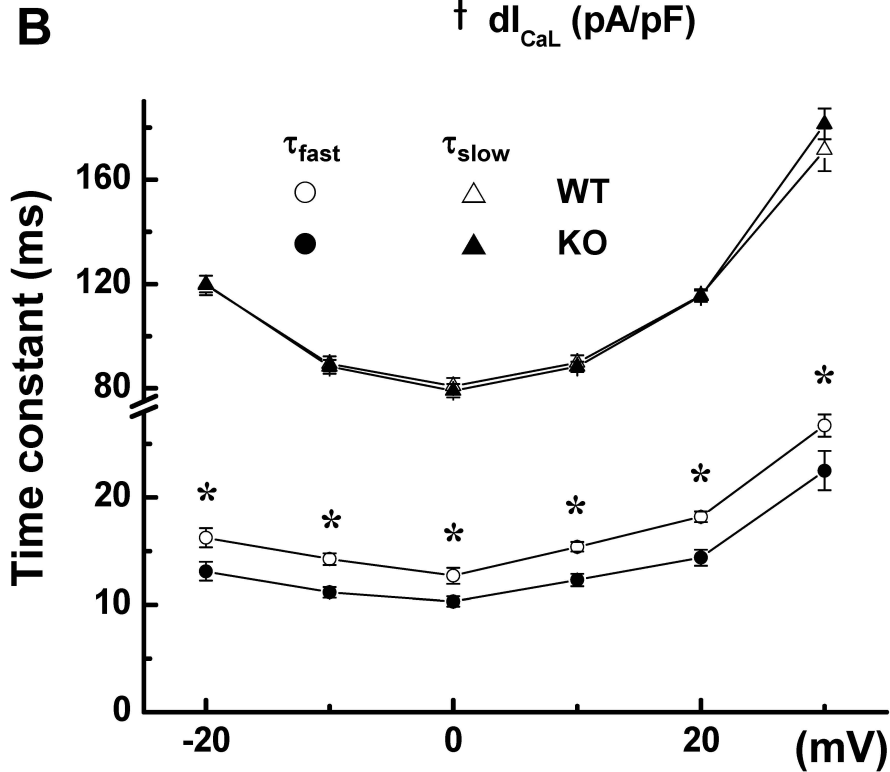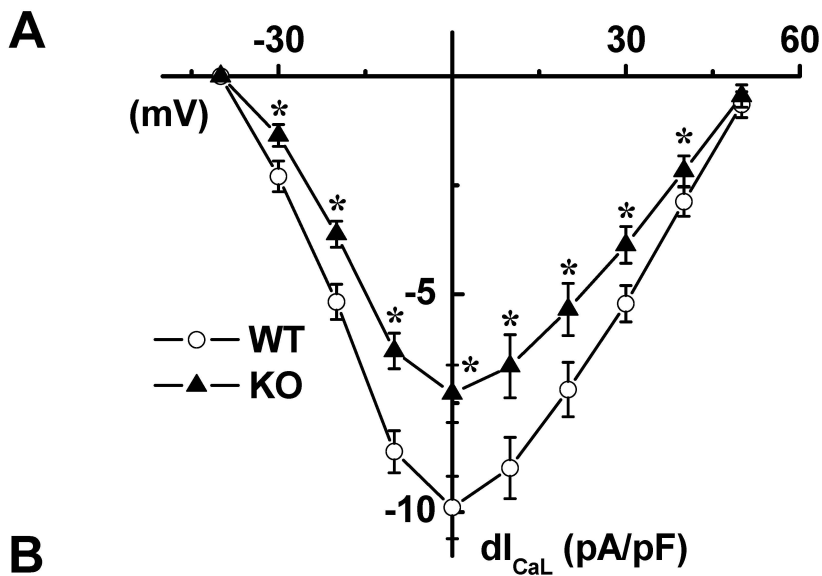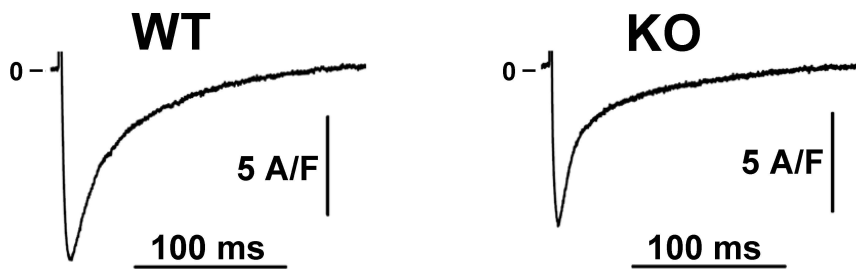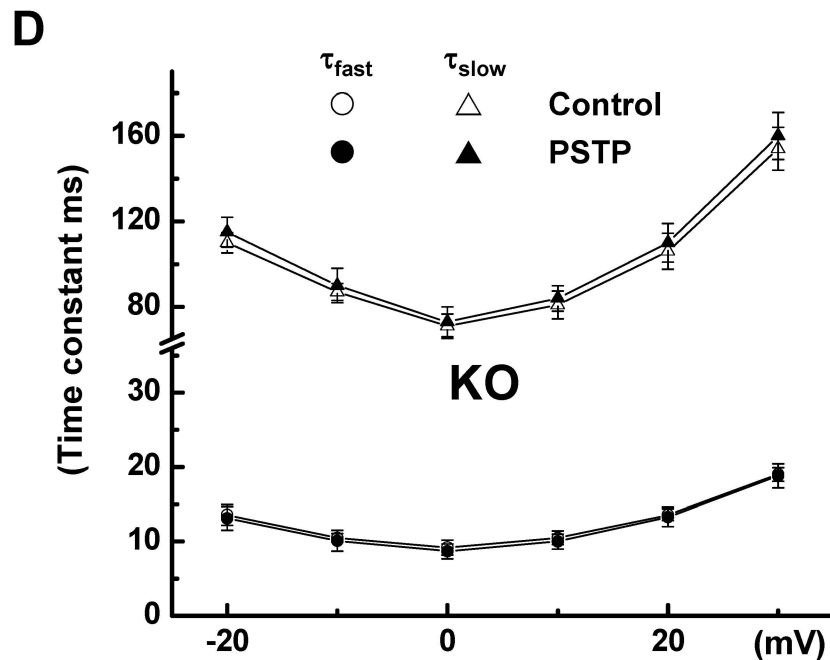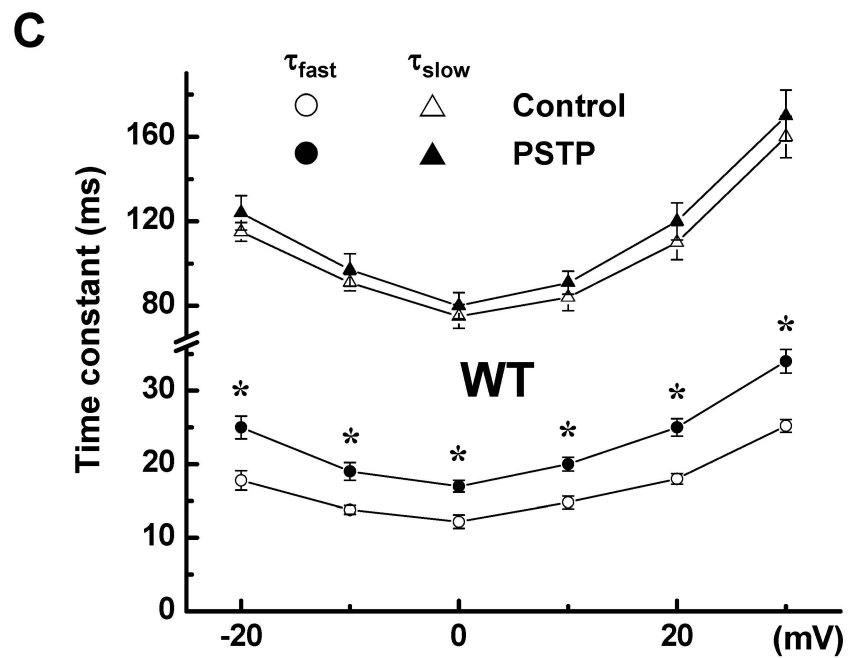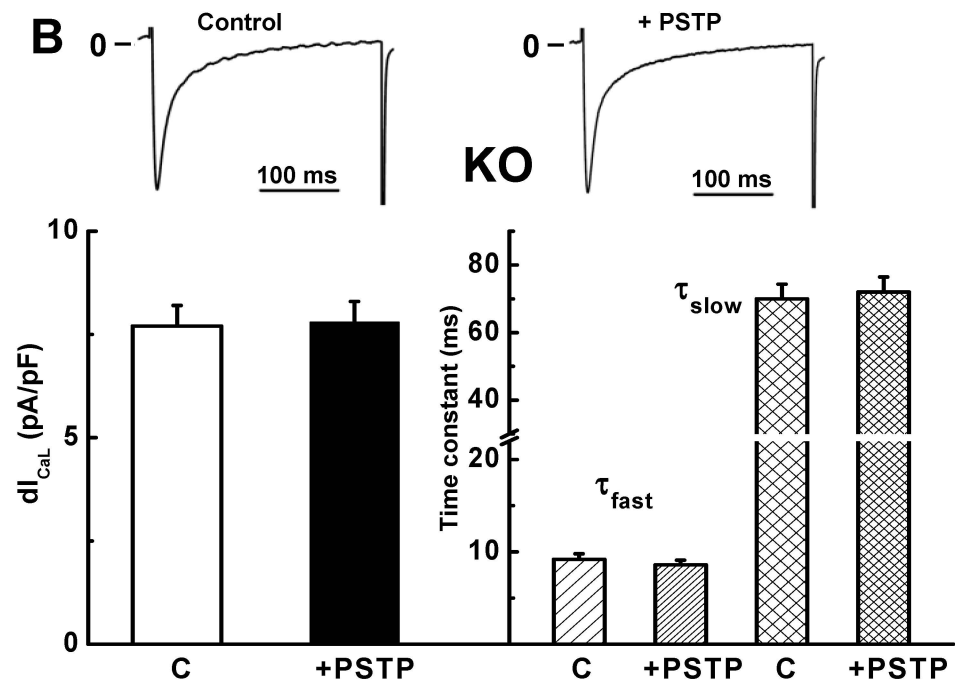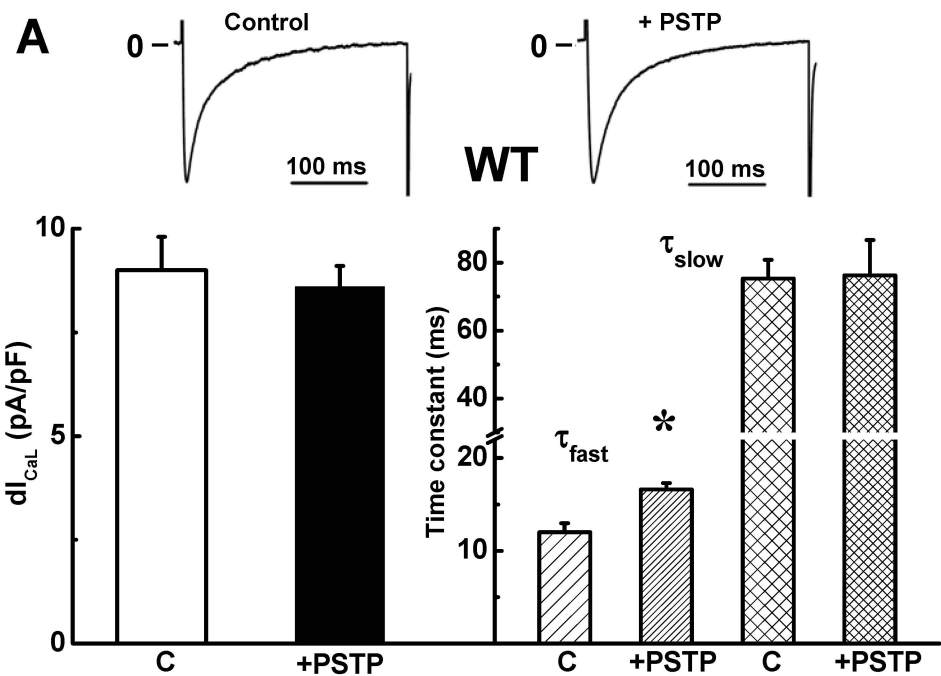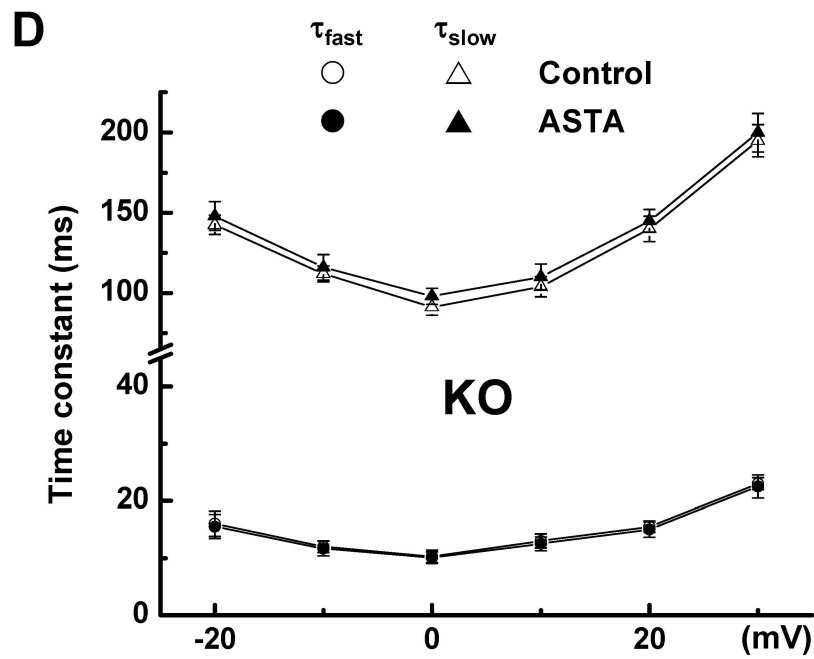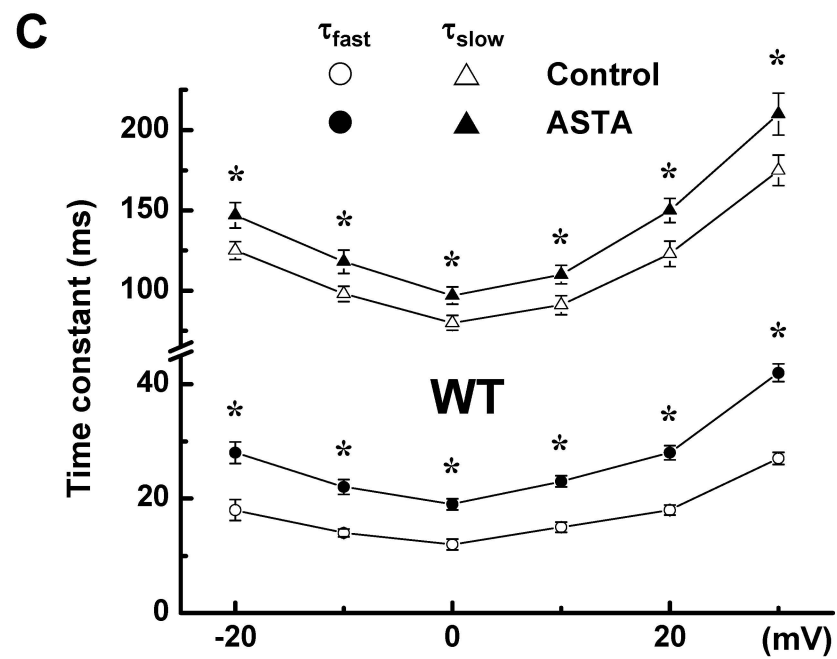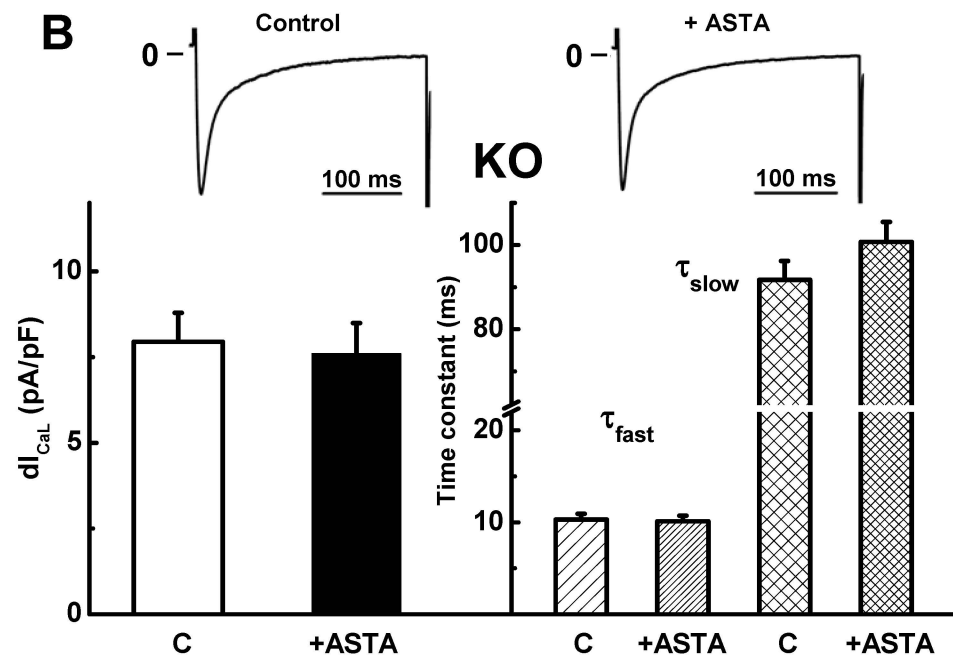
Figure 1. Interaction between the recombinant β₂-subunit and the C-terminal portion of ahnak1 containing either the PSTP- or ASTA-sequence. A) Different mixtures of 0.35 µM recombinant β₂-subunit and variable amounts of the C-terminal ahnak1 fragments 188-PSTP (filled circles) or 188-ASTA (open circles) were centrifuged to the sedimentation equilibrium for 16 h at 10°C. B) Surface plasmon resonance measurements demonstrating real time β₂-subunit binding to the C-terminus of ahnak1 containing either the PSTP-sequence (solid line) or the ASTA-sequence (dashed line) at 25 °C. The ahnak1-derived fragments were immobilized at parallel lanes of a CM5 biosensor chip at 700 response units. Recombinant β₂-subunit (2 µM) was passed at 20 µl/min over the surface (Association) followed by running buffer alone (Dissociation). Note 188-PSTP exhibits higher binding affinity and capacity for the β₂-subunit in equilibrium binding experiments.

Figure 2. Effects of 188-PSTP and 188-ASTA on I_{CaL} of rat ventricular cardiomyocytes. A,B) I_{CaL} was elicited by 200-ms depolarization to 0 mV from a holding potential of –80 mV. Superimposed current traces recorded in rat ventricular cardiomyocytes under control conditions (Control), or intracellularly dialyzed with 100-nM 188-PSTP (PSTP) or 5-µM 188-ASTA (ASTA). Running integrals of QCa^{2+} attributed to I_{CaL} recordings are presented below. C) Voltage-dependency of the inactivation time constants, τ_{fast} and τ_{slow} in the same experimental conditions. n = 17 Control, 8 PSTP or 6 ASTA from at least 4 hearts. * p < 0.05 with respect to control.

Figure 3. Effects of 188-PSTP and 188-ASTA on I_{BaL} of rat ventricular cardiomyocytes. A) The inward current carried by Ba^{2+}, I_{BaL} was elicited by 300-ms depolarization to 0 mV from a holding potential of –80 mV. Superimposed current traces recorded in rat cardiomyocytes under control conditions (Control), or intracellularly dialyzed with the C-terminal ahnak1 fragments 188-PSTP or 188-ASTA (10 µM each). B) Voltage-dependency of the inactivation time constants, τ_{fast} and τ_{slow} in the same experimental conditions. Note that at –20 mV the currents were fitted by only one inactivation time constant. n = 12 Control, 6 PSTP or 6 ASTA from at least 4 hearts. * p < 0.05 with respect to control.

Figure 4. Phenotype of ahnak1-deficient cardiomyocytes. A) Total cardiac tissue lysates from wild-type (WT) and ahnak1-deficient mice (Ahnak1-KO) were subjected to SDS-PAGE and Western-blot analyses using an affinity-purified antibody generated against the head portion of ahnak1. The lower panel shows the Coomassie-stained myosin heavy chain (MyHC) as loading control. B) Phase contrast images of representative cardiomyocytes isolated from 6 months old wild-type and ahnak1-deficient mice.

Figure 5. I_{CaL} kinetics in cardiomyocytes from wild-type and ahnak1-deficient mice. A) Current-voltage relationships established in wild-type (WT) and ahnak-deficient (KO) mice ventricular cardiomyocytes. I_{CaL} is expressed as current density (pA/pF). Inset: representative Ca^{2+} current tracings. B) Voltage-dependency of the inactivation time constants, τ_{fast} and τ_{slow} in WT and KO cardiomyocytes. n = 22 WT and 38 KO cardiomyocytes from at least 6 WT and 12 KO hearts. * $p < 0.05$ with respect to control.

Figure 6. Effects of 188-PSTP perfusion on I_{CaL} characteristics of cardiomyocytes from wild-type (A, C) and ahnak1-deficient (B, D) mice. A, B) Bar graphs comparing peak inward current, I_{CaL} and inactivation time constants, τ_{fast} and τ_{slow} in control conditions and in the presence of 10-μM intracellular 188-PSTP. Inset: representative Ca^{2+} current tracings. Currents were normalized to maximal peak inward current. C, D) Voltage-dependency of the inactivation time constants, τ_{fast} and τ_{slow} in the same experimental conditions. n = 9 WT and 9 KO, and 9 WT and 7 KO cardiomyocytes in control and PSTP, respectively derived from at least 4 animals per group. * $p < 0.05$ with respect to control.

Figure 7. Effects of 188-ASTA perfusion on I_{CaL} characteristics of cardiomyocytes from wild-type (A, C) and ahnak1-deficient (B, D) mice. A, B) Bar graphs comparing peak inward current, I_{CaL} and inactivation time constants, τ_{fast} and τ_{slow} in control conditions and in the presence of 10-μM

intracellular 188-ASTA. Inset: representative Ca^{2+} current tracings. Currents were normalized to maximal peak inward current. C, D) Voltage-dependency of the inactivation time constants, τ_{fast} and τ_{slow} in the same experimental conditions. n = 8 WT and 8 KO, and 5 WT and 7 KO cardiomyocytes in control and ASTA, respectively derived from at least 4 animals per group. * p < 0.05 with respect to control.

Figure 8. Expression of the Ca^{2+} channel subunits α_{1C} and β_2 in ahnak1-deficient and non-transgenic cardiomyocytes. Western-blot analyses demonstrating β_2-subunit (A) and α_{1C}-subunit (B) protein levels in the total cardiac membrane protein fraction of ahnak1-KO and wild-type mice compared to recombinant β_2-subunit (96-kDa) and α_{1C}_II-III loop (55-kDa). C) Detection of β_2-subunits in total heart proteins (30 µg) prepared from the rodent models as indicated (left panel) and in the rat heart cytosolic fraction before and after pull-down with the α_{1C}_I-II loop (right panel).

Supplemental Material:

Patch clamp experiments

Electrode resistance was between 0.9 - 1.1 MΣ. C_m was estimated by applying 10 ms/2mV hyperpolarizing pulses from a holding potential (HP) of –80 mV. Capacitive spikes were fitted to a simple exponential and C_m was calculated according to:

$$C_m = \tau_m \cdot I_0 / V_m (1 - I_{ss} / I_0)$$

where ϑ_m is the membrane time constant, I_0 is the maximal amplitude of the capacitive current spike, I_{ss} is the "steady-state" current at the end of the 10-ms pulse and V_m is the amplitude of the voltage step (2 mV). The series resistance (R_s) with the cell membrane was estimated according to $R_s = \vartheta_m / C_m$. Uncompensated series resistance was 3.9 ± 0.3 MΩ (n = 20) in rat cardiomyocytes and 3.7 ± 0.3 MΩ (n = 65) in mouse cardiomyocytes. R_s could be electronically compensated up to 50% without ringing. In order to isolate I_{CaL}, K^+-currents were blocked by Cs^+ (intracellular and extracellular; see below). In rat ventricular cardiomyocytes the fast inward Na^+ current (I_{Na}) was blocked with tetrodotoxin (50 µM). The composition of the standard extracellular solution was (mM): 117 NaCl, 20 CsCl, 2 $CaCl_2$, 1.8 $MgCl_2$, 10 glucose, 10 HEPES, pH 7.4. The pipette ("intracellular") solution contained (mM): 130 CsCl, 0.4 Na_2-GTP, 5 Na_2-ATP, 5 Na_2-creatine phosphate, 11 ethyleneglycol-bis-(-aminoethyl ether) N,N,N',N'-tetraacetic acid (EGTA), 4.7 $CaCl_2$ (free Ca^{2+} :120 nM); 10 HEPES; pH was adjusted to 7.2 with CsOH. The Ca^{2+} current was routinely evoked with 200-ms depolarising pulses to 0 mV applied from a –80 mV HP every 4 s. In mouse ventricular myocytes I_{CaL} was monitored by a two-step voltage-clamp protocol: from a –80 mV HP a 50-ms step pulse to –40 mV to fully inactivate I_{Na}, a 300-ms step to 0 mV was applied. The double-pulse interval was 4 s. In both cases, peak I_{CaL} was measured as the difference between maximal inward current and the current level at the end of the depolarising pulse and normalized to membrane capacitance (C_m) to estimate I_{CaL} density.

Current-to-voltage (I-V) and availability curves were obtained in rat cardiomyocytes according to previously established standard double-pulse protocols {Alvarez, 2004 #1}. In mouse cardiomyocytes the following voltage clamp protocol was used: every 8 s, from a –80 mV HP a 50-ms step pulse to –40 mV was applied followed by 300-ms prepulses from –50 to +60 mV. After a 5-ms gap at –40 mV,

each prepulse was followed by a fixed 300-ms test pulse to 0 mV. I-V curves were obtained from currents elicited during the prepulses. Availability was estimated by normalizing current amplitude at the test pulse by the current recorded as a function of prepulse potential. The experimental points between –50 and 0 mV were fitted to a Boltzmann function:

$$I / I_{max} = (1 + \exp ((V_p - V_{0.5}) / s))^{-1}$$

where V_p is the prepulse potential, $V_{0.5}$ is the half-availability potential and s the slope factor. Ca^{2+} current inactivation was analysed by fitting current traces to double exponentials {Alvarez, 2004 #1}. The amount of Ca^{2+} charges (QCa^{2+} in pC) entering the cell during a depolarising pulse to 0 mV was estimated by integrating the current trace from the return to the baseline just after the capacitive transient to the end of the voltage-clamp pulse just before the capacitive transient, and was normalized to membrane capacitance (pC/pF).

In some experiments with rat cardiomyocytes, on applying 300-ms duration pulses currents were first recorded with Ca^{2+} as charge carrier and then after equimolar Ba^{2+} substitution. Under these conditions I_{BaL} inactivation time course could be well fitted by two exponentials over the membrane potential range studied, except at -20 mV where a single exponential was the best fit. The amount of Ba^{2+} charges was estimated by integrating the current trace from the zero current during a 300-ms depolarization to 0 mV.